FE MODELLING OF THREE DIMENSIONAL STAGGERED BACKWARD METAL FLOW FORMING PROCESS

Prabas Banerjee[1], Nirmal Baran Hui[1], Mithilesh K Dikshit[2], Saikat Som[3]

[1]"Department of Mechanical Engineering, National Institute of Technology, Durgapur, West Bengal – 713209, India
[2] Department of Mechanical Engineering, Institute of Infrastructure Technology Research and Management, Ahmedabad, India
[3]Department of Mechanical Engineering, Kannad Institute of Engineering and Technology, Durgapur, West Bengal-713209

Corresponding author: Prabas Banerjee, prabasbanerjee@gmail.com

Abstract: A three-dimensional Finite Element (FE) model for a backward flow forming process is developed using ABAQUS simulation software. Forming parameters such as feed speed ratio, percentage reductions, and roller geometries on the stresses, forces, power, and dimensions of flow formed tubes are studied. A comparison between the traditional theoretical formulations and simulated forces is made. The impact of feed speed ratios and percentage reduction on out of roundness of flow formed tubes are studied and compared with experimental results. The closeness of the estimated power to the experimental power available in the literature shows that the developed simulated model is promising and robust.

Key words: flow forming, AA6082, finite element modelling, forces components, out of roundness

1. INTRODUCTION

Metal flow forming is primarily used for the fabrication of long cylindrical pipes. In this process, the thickness of the tube is reduced, keeping the internal diameter unchanged [1-3]. The metal flow forming process finds application in defense and aerospace industries. The flow formed components are used as rocket motor shells, gas turbines, and airframe hardware. Productivity in the flow forming process is highly influenced by tooling and multiple reductions. In this process, a simple tooling arrangement and multiple reductions lead to increased productivity [4]. Multiple reductions are generally achieved by rolling forces and roll power. Various researches have been done to predict rolling forces and roll power. Dimensional accuracy is one of the parameters which characterize the quality of flow formed products. Hayama and Kudo [5] experimentally predicted rolling forces and the dimensional accuracy in the flow forming process. Nagarajan et al. [6] had studied the deformation zone and deformation forces to achieve the desired dimensional accuracy of the flow-formed products. The authors also describe the complexities of the deformation zone. Singhal et al. [7] used analytical formulations to determine the flow forming forces and power required during the deformation process. Various researchers have employed finite element (FE) methods to model the flow forming process. Using a cylindrical tube with one roller, Wong et al. [8] investigated the axial and radial forces. The authors had concluded that an explicit dynamic solver is best suited. Hua et al. [9] investigated the role of stresses, strains, and developed forces in tube spinning processes. The axial stagger of rollers wasdid not influence the roll forces. Xia et al. [10] had done a comparative study of roll forces between axisymmetrical and non-axisymmetrical tubes in the flow forming process by varying the angle of revolution of the rollers around the tube. It was concluded that the roller force proporationally increased with increase in percentage reduction and feed rate for both the type of tubes. Wong et al. [11] used FE-based simulation to investigate the reduction percentage in the material flow using DEFORM 3D. Parsa et al. [12] studied the contact geometries, radial, tangential and axial stress, and strain distribution beneath the roller and workpiece contact zone in flow forming using explicit solver. The explicit solver took less computational time as compared to the implicit solver. Razani et al. [13] investigated the effect of mandrel speed, a percentage reduction, and feed rate on the hardness of flow-formed cylindrical tubes using the response surface method. The authors had observed that the hardness of flow formed tube proportionally increased with an increase in mandrel speed percentage reduction. Xu et al. [14] studied the eccentric forces developed by the rollers on the mandrel. They also studied the effect of such forces on the dimensional accuracy of flow formed cylindrical tubes. They stated that non-periodic circumferential stress distribution was observed due to non-uniform roller distribution. Song et al. [15] also studied the diametral growth in cylindrical tubes by the forward flow forming process. They stated that improving lubrication diminishes diametral growth.

Various researchers have employed FE based simulation software such as ANSYS and ABAQUS to model and study the influence of different parameters in flow forming processes [16-18]. Shinde et al. [19] studied the effect of feed rate and reduction ratio on MDN 250 maraging steel in the backward flow forming process. They studied the stress and strain distribution with the help of the ABAQUS simulation software. They reported that high magnitude stresses and strains due to material build-up in front of rollers.

In the present research, a FE based simulation model is developed for the backward metal flow forming process using ABAQUS simulation software. Various forming parameters such as roller geometry, feed speed, percentage reduction, and axial staggered arrangement of rollers are considered to study the stress distribution, forming forces, and power consumed during the process. The influence of input parameters on the response out of roundness of flow formed tubes is analyzed and compared with the experimental findings.

2. PHYSICAL DESCRIPTION AND FE BASED MODEL

Deformation of preform in backward metal flow forming process is done by the compressive forces of the rollers. Multiple rollers are used to achieve multi reduction in one pass. In this research, three rollers are used. The rollers are arranged in an axial staggered manner along the preform's axial length shown in Figure 1. An axisymmetric view of the preform is represented in Figure 1(a) with an initial and final thickness of T_0 and T_f, respectively. The distance between the first and the last roller is represented by *a*, while the axial distance between the second and the last roller is represented by *b* in Figure 1(a). At the same time the reduction caused by the first roller is shown as T_1 while the reduction caused by second and the last roller is represented as T_2 and T_f respectively. The difference between the original thickness and the final thickness is the infeed or the reduction ratio of the forming process. The unit of infeed is mm. Thus, the axial stagger arrangement enables multiple reduction during one pass of the rollers. Rollers are placed circumferentially along the preform at an angle of 120º from each other. Figure 1 (b) shows the rotational stagger arrangement of three rollers. The preform is mounted on a mandrel. The rollers are mounted on a saddle that is provided axial velocity along the axis of the preform.The inside diameter of the preform is the same as the diameter of the mandrel. The mandrel is provided a rotational velocity. Since the preform is attached to the mandrel by means of stripper ring, the preform also rotates with the same velocity. The ratio of the axial velocity of the roller and the rotational velocity of the preform is termed as the feed speed ratio. The unit for feed speed ratio is mm/rev. The inside surface of the preform remains unaltered, which is one of the significant advantages of this process. As the roller moves, the preform's thickness is reduced by the compressive action of the roller, and the mandrel started flowing in the axially forward direction. The reduction in the preform thickness allows elongation along the axial direction, opposite to that of the roller movement.

To develop the simulation model, the FE model is divided into three sections. The first section discusses the definition of various parts in the model; the next section discusses the assembly of the parts, and the last section explains about the boundary conditions of the model and type of solver used in the FE model. In the first step, various part geometries are used. The model consists of four parts, namely the mandrel, rollers, stripper ring, and perform. The parts are sketched using AUTOCAD and finally imported to ABAQUS for further processing. The preform has an inner diameter of 120 mm, a thickness of 7 mm, and an axial length of 180 mm. The diameter of the mandrel is same to the inner diameter of the preform. It is considered as the deformable part in the FE model, which is made of AA 6082 alloy. The flow stresses (σ)is regarded as given in equation (1)

$$\sigma = K\varepsilon^n, \tag{1}$$

where ε is the strain, K is material constant, and n is strain hardening exponent. The material properties of the preform is depicted in Table 1 [20].

Table 1. Material properties of the preform

Part	Preform
Material	AA6082
Density (kg/m^3)	2750
Young's Modulus (GPa)	70
Poisson's Ratio	0.33

The rollers, mandrel, and the stripper ring are made up of AISI die steel material. In the simulation these are considered as rigid bodies for saving computational time. The stripper ring prevents the deformation of the material in the direction of roller movement. The three rollers are arranged in axial and rotational stagger manner. The axial stagger arrangement is made to facilitate multiple reductions in one pass. In the developed model, the distance between the first roller and the last roller is 9.5 mm. The geometries of the rollers include the entry angle, nose radius, and exit angle. The geometrical values of the three rollers are shown in Table 2. Similar roller geometries were used by Shinde et al. [19] to develop a FE model. The parametric value of the angle, nose radius and exit angle is selected based on the previous research [13, 21].

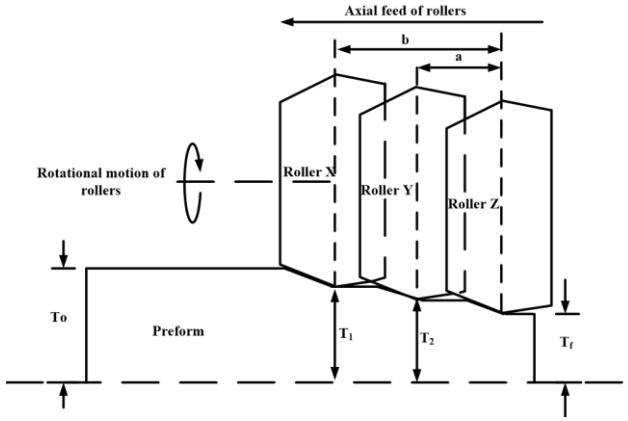

(a)

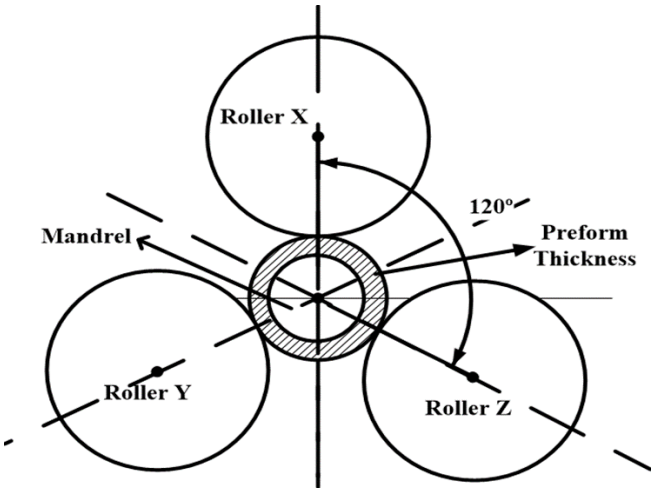

(b)

Fig.1. Schematic representation (a): Axial stagger of rollers (b) rotational stagger of rollers

Table 2. Roller Dimensions

Part Name	Entry Angle, α (º)	Nose Radius, *r* (mm)	Exit Angle, β (º)
Roller 1	15	4	5
Roller 2	24	4	12
Roller 3	30	4	12

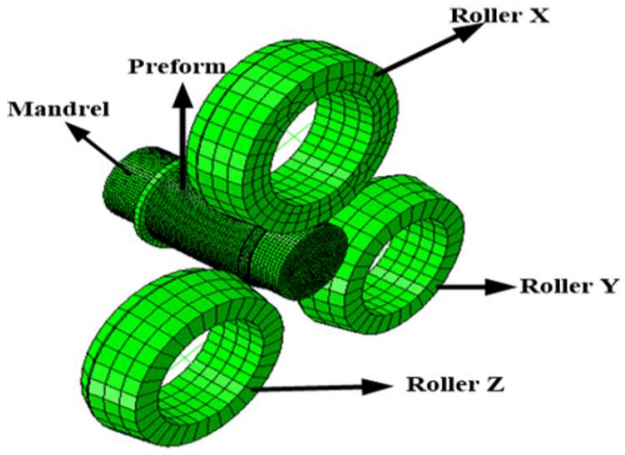

(a)

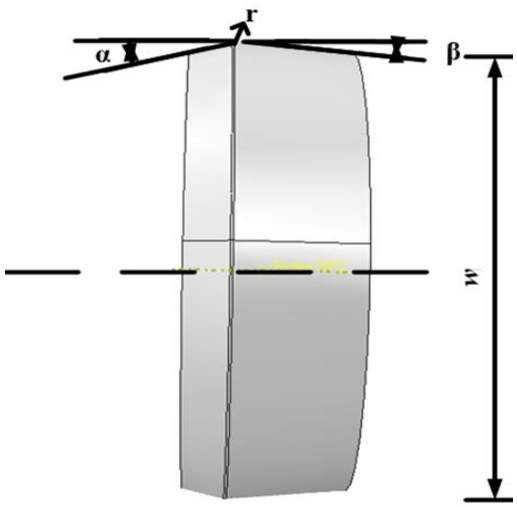

(b)

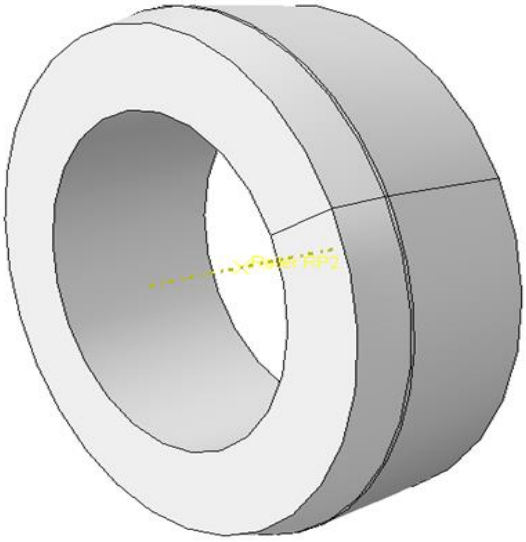

(c)

Fig. 2. Parts of the simulation model (a) complete model (b) geometry of the roller (c) x-y plane view of the roller

The second part is the assembly step of the part geometries. In this step, the part geometries are assembled. Figure 2(a) shows the assembly of the four different part geometries used in the model. Figure 2(b) and Figure 2(c) depicts the roller geometries considered in the model. In the assembly section, contact between the rollers and the preform is established. The feed for the three rollers is different, and the highest feed is provided to the last roller. The stripper ring constricts material so that the elongation takes place in the opposite direction of the roller movement. The interaction between the roller and the preform as well as the interaction between the preform and the roller is defined. The surface of the roller is considered as the master surface, and the top surface of the preform is considered as the slave surface [22]. Two types of contact are available in ABAQUS (node to surface and

surface to surface) [23]. Node to surface contact condition allows penetration of rigid bodies into deformable bodies, which is undesirable [10]. Therefore, a surface to surface contact is selected for defining the contact surfaces between individual parts. A friction factor of 0.1 between the rollers and the preform is considered in the developed model [21]. In the modeling of the flow forming process C3D8R type of element is selected to define the preform. The C3D8R element is a general-purpose linear brick element with reduced integration (1 integration point). The shape functions are the same for the C3D8R element. The integration point of the C3D8R element is in the middle of the element [24]. Thus, small elements are required to capture a stress concentration at the boundary of the structure. Seed size of 0.001 is considered in developing the FE model of the flow forming process.

The boundary conditions are defined at the last step of the model where, the movement of the rollers along the axial direction of the preform is provided. No rotational condition is given to the preform along y and z-direction. All the other directions of the preform are kept free. The mandrel provides the rotational motion of the preform. A reference point is defined for the stripper ring, and its movement is constrained in all directions except along the x-direction so that it could be rotated with the help of mandrel. The implicit method is not suited to solve problems in which there is a frequent change in the contact condition. Such issues can be addressed by an explicit method which is governed by the equation (2):

$$M\ddot{u}=P-I \qquad (2)$$

where M is the mass, u is nodal displacement, P is the external load vector, and I is the internal load vector. Time increment depends on the element dimension and not on the complexity of the analysis. The acceleration of the node depends only on the mass of the element and the net force acting on it, which makes nodal calculation less expensive. The explicit analysis is conditionally stable, and the time step is limited, which is a major drawback of this technique. Material density and loading speed can be increased artificially to monitor the incremental forming process.

3. RESULTS AND DISCUSSIONS

In this section, stresses, forming forces, power and dimensional accuracy of the tubes are studied. Important input parameters such as feed speed ratio, axial stagger of the rollers, and percentage reduction are considered. The effect of the input parameters are studied on the above mentioned output parameters of the simulated model.

3.1 Stresses and strains at a different feed speed ratio

Stresses are studied in this subsection. Percentage reductions of 10, 20, 30, 40 and 50 are shown in Figure 3(a-e) respectively for feed speed ratio of 0.7 mm/rev.

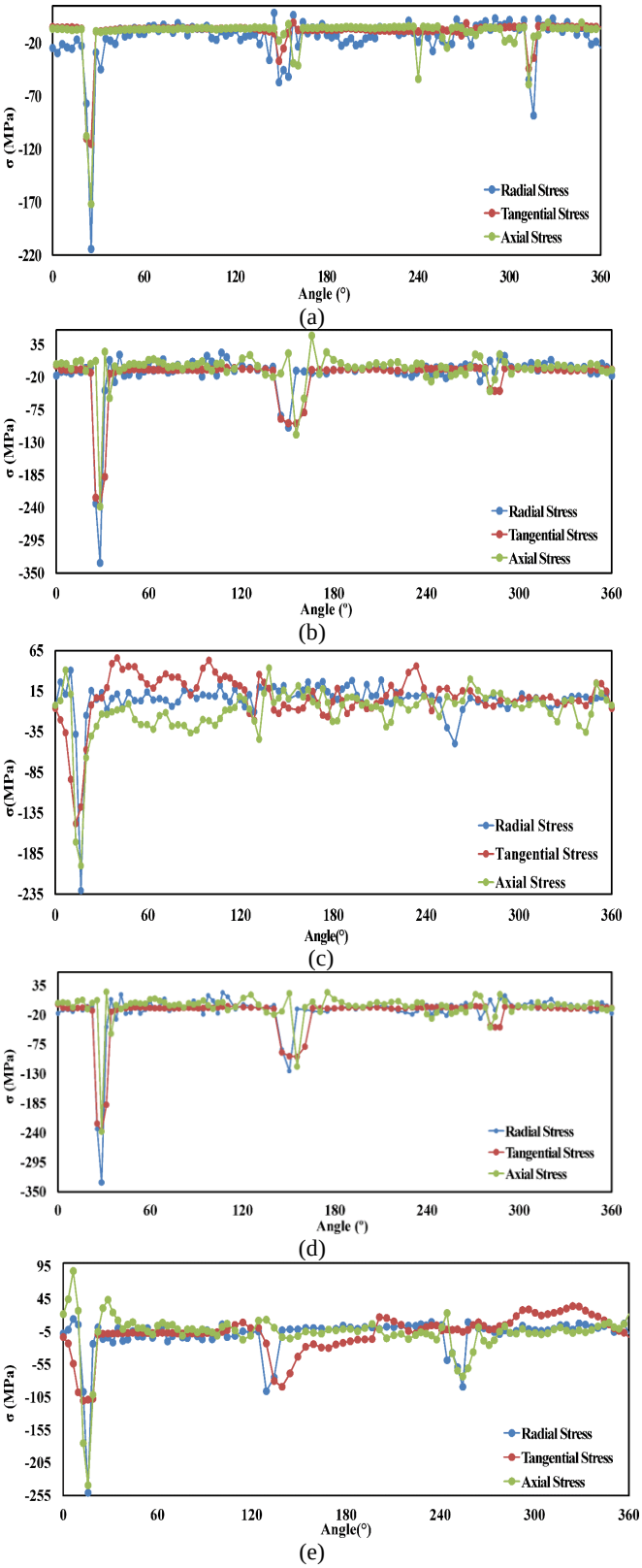

Fig. 3: Stresses under the roller at feed speed ratio of 0.7 mm/rev. (a) 10% (b) 20% (c) 30% (d) 40% and (e) 50% reduction

The stress for different percentage reductions (0.7 and 0.8 mm/rev) are shown in Figures 3 (a-e) and Figures 4(a-e), respectively. From the Figures 3(a-e) and Figures 4(a-e), the radial stresses are compressive, and they are highest among the other two stress components (axial and tangential). The stresses are measured along the circumference of the preform. The initial point of the circumferential length is selected close to the first roller. The stress under the first roller is highest because it makes initial contact with the preform surface. Figures 3(a-e) and Figures 4(a-e) shows that the regions close to the rollers experience more significant stress than the other areas that are not in contact with the roller. It suggests the incremental characteristic of this complex forming process. This is due to the fact that stresses are only obtained at the contact between the roller and the preform. However, at some locations, non-zero values of stresses are observed, which is due to some computational and approximation errors. The localized stresses suggest that during contact between the roller and perform, only a small area is deformed. The stresses also indicate that there are continuous changes in the contact area. This happens due to instantaneous engagement and disengagement between the roller and preform. In Figures 3(a-e) and Figures 4(a-e), the axial and tangential stresses vary at different feed speed ratios for the same percentage reduction. This is due to the increase in the axial feed of the rollers as more elements are swept under the rollers. Also, the contact between the roller and the preform changes frequently. From this analysis, it could be ascertained that the radial stress is the highest among the three components of stress. The feed speed ratio and percentage reduction. The components of stress increase with an increase in the feed speed ratio and percentage reduction.

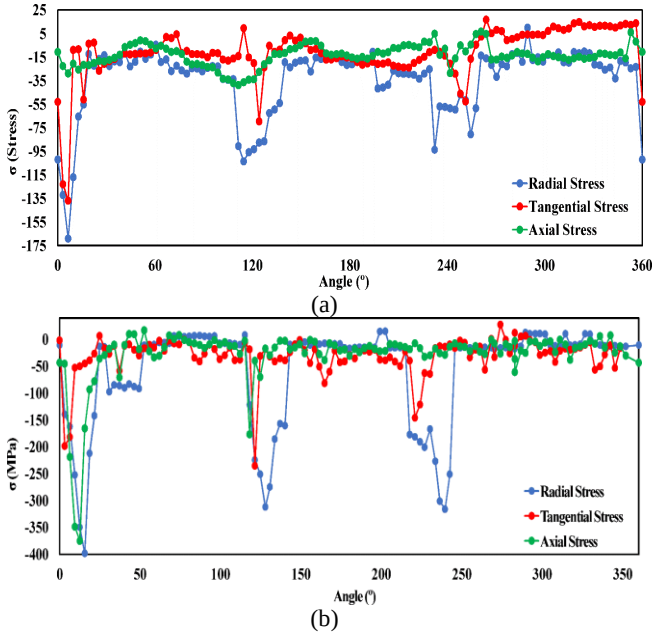

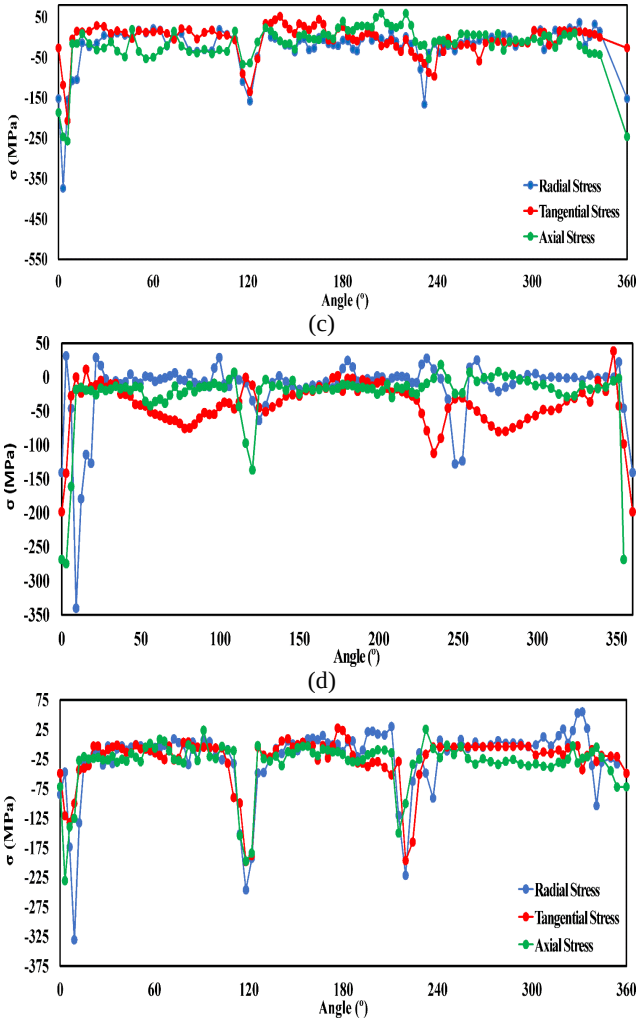

Fig. 4. Stresses under the roller at feed speed ratio of 0.8 mm/rev. (a) 10% (b) 20% (c) 30% (d) 40% and (e) 50% reduction

3.2 Comparison of the different components of forming forces

The simulated forming forces are compared with the theoretical models of Kobayashi [25], Thamasett [26], Chen [27], and Ma's [28]. One of the objectives of this research is the determination of forming forces. The forming forces are divided into radial, axial, and tangential forces. In this research, the simulated forces at different percentage reduction and different feed speed ratios are studied. The forces obtained from the FE model, theoretical models at a different feed speed ratio of 0.7 mm/rev, 0.8 mm/rev is shown in Figure 5, and Figure 6, respectively. The forces obtained from the FE model are compared with the forces obtained from theoretical models Kobayashi [25], Thamasett [26], Chen [27], and Ma [28]. The components of forces (radial, axial, and tangential) and the ratio of radial to axial force and ratio of radial to tangential forces are shown in Figure 5 and Figure 6, respectively.

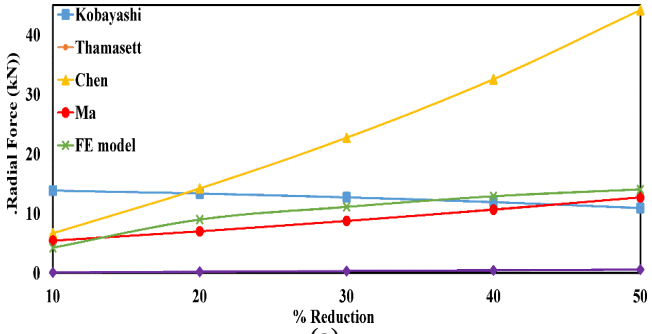

(a)

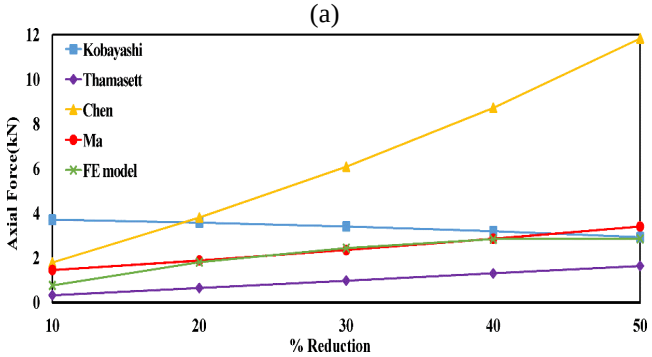

(b)

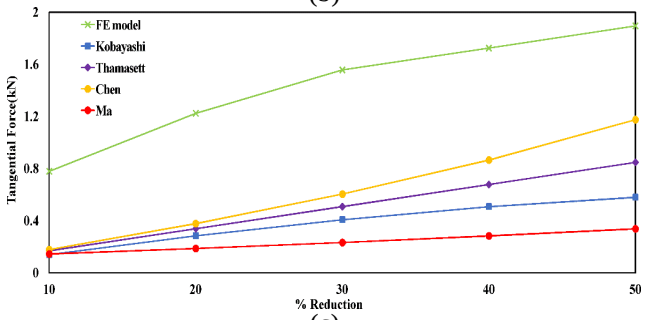

(c)

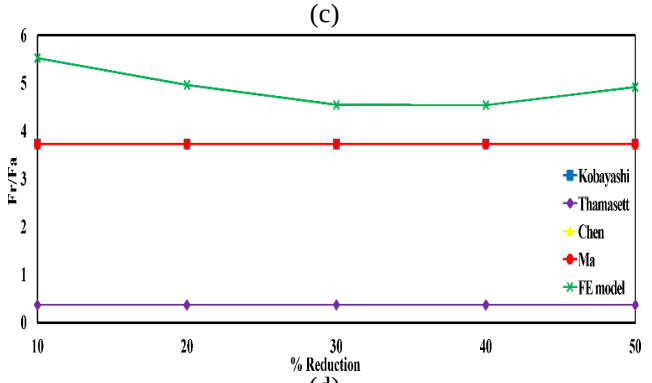

(d)

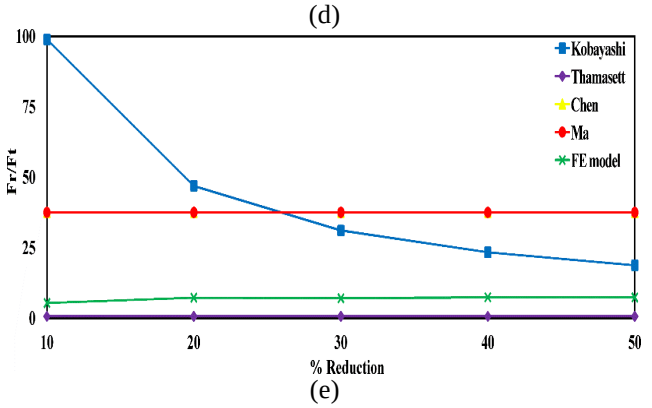

(e)

Fig. 5. Comparison of forces with theoretical forces at a feed-speed ratio of 0.7 mm/rev (a) Radial forces (b) Axial forces (c) Tangential forces (d) ratio of radial to axial forces (e) ratio of radial to tangential forces respectively

The obtained simulated radial forces are compared with the theoretical model of Kobayashi [25], Thamasett [26], Chen [27], and Ma [28], as shown in Figure 5(a) and Figure 6(a) at different feed speed ratio of 0.7 mm/rev and 0.8 mm/rev respectively. The radial force at both feed speed ratio of 0.7 and 0.8 mm/rev increases with an increase in the percentage of reduction. The simulated radial forces show the same increasing trend as that of Chen's [27] and Ma's [28]. Also, for both the feed speed ratios of (0.7 and 0.8) mm/rev, a close nearness is observed with the forces derived from Ma's [28] theoretical formulations, as observed from Figure 5(a) and Figure 6(a). In the analytical formulation presented by Ma [28], roller geometry is considered. The radial force compresses the material of the preform. The deforming material is constricted by the surrounding material, which is not under the roller. Some material escapes along the axial direction and some amount of the material in the circumferential direction. There is an accumulation of material in front of the roller. The material built up in front of the roller and the material forming along the circumferential length of flow formed tube causes variation in thickness. Such uneven material distribution causes a change in the mean thickness of flow formed tubes. The findings from this research are in line with the previous findings from the literature [3], where the radial forces increase with an increase in feed speed ratio and percentage reductions.

Figure 5(b), Figure 6(b) shows the axial forces obtained from the developed FE model and the from the theoretical formulations at feed speed ratio of 0.7 mm/rev, 0.8 mm/rev respectively for different percentage reductions. The axial forces increase with an increase in feed speed ratio for the same percentage reductions. The axial force determines the required feed force, which helps in the elongation of material in the axial direction. The simulated axial forces show a similar increasing trend as that of Chen's and Ma's [28] theoretical formulations. However, close nearness of the simulated axial forces is reported to that of Ma's theoretical formulations. Kim et al. [21] suggested that a material build-up influences the axial force in front of the rollers. The material build-up is influenced by roller geometry. In Ma's [28] theoretical model, roller geometry is taken into consideration for the determination of forming forces. In the developed FE model, roller geometry is defined in the form of entry angle, nose radius, and exit angle. Thus a close nearness of the simulated axial forces is obtained with that of Ma's [28] theoretical formulations.

Figure 5(c) and Figure 6(c) shows the comparison of simulated tangential forces at 0.7 mm/rev, 0.8 mm rev, respectively, with forces obtained from different theoretical formulations. It is observed that the

simulated tangential forces overshoot the theoretical model of Kobayashi [25], Thamasett [26], Chen [27], and Ma [28]. The tangential forces arise due to the rotation of the elements of the preform. Although the simulated forces overshoot the theoretical models in the literature, the trend of the simulated forces matches with the theoretical models. The tangential force compels the material flow along the circumferential direction due to the constraint of material flow in another direction. Chen et al. [27] neglected the friction between the tool and workpiece, while in Ma's [28] method, the shearing factor was used to denote the ratio of friction force versus the shear resistance. The tangential force is the lowest among the simulated radial and axial forces.

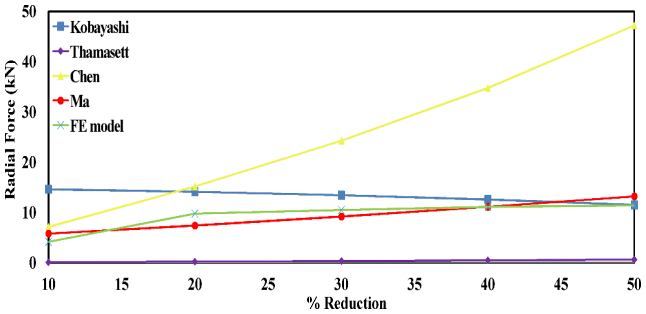

(a)

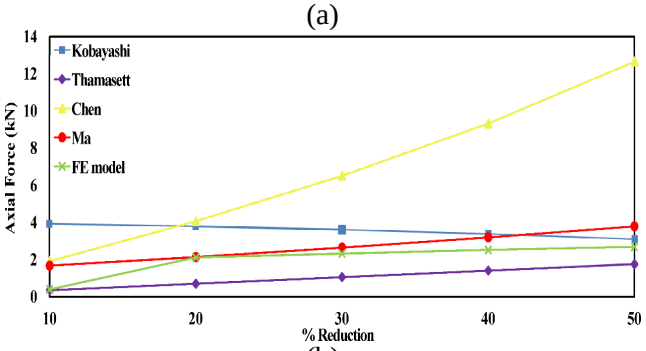

(b)

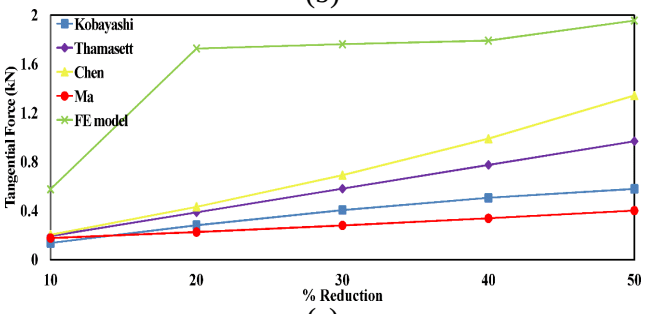

(c)

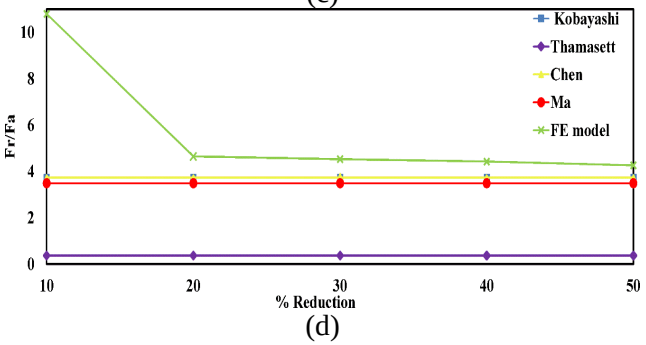

(d)

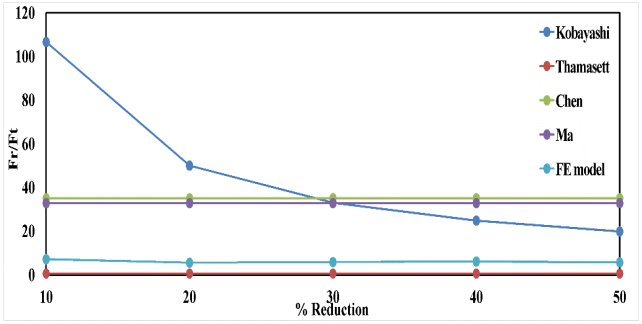

(e)

Fig.6. Comparison of forces with theoretical forces at a feed-speed ratio of 0.7 mm/rev (a) Radial forces (b) Axial forces (c) Tangential forces (d) ratio of radial to axial forces (e) ratio of radial to tangential forces

Figure 5(d) and Figure 6(d) shows the ratio of radial to axial forces at a feed speed ratio of 0.7 mm/rev, 0.8 respectively.

Figure 5(e) and Figure 6(e) shows the ratio of radial to tangential forces at a feed speed ratio of 0.7 mm/rev, 0.8 mm/rev, respectively. The ratio of the forces suggests that with a change in the percentage reductions, the ratio of simulated forces changes. At the same time, the ratio of forces obtained from the theoretical model mostly remains unchanged. This suggests that the forces derived from the FE model are realistic and robust.

3.3 Comparison of simulated power with experimental results

Nagarajan et al. [6] experimentally determined the power required during the flow forming of aluminum tubes. An axial feed of 1.5 mm/rev was used for the rollers, while a rotational velocity of 500 RPM was considered for the mandrel. In this simulation, a feed speed ratio of 0.7 and 0.8 mm/rev was assumed. Many researchers have calculated the components of the forming forces using analytical approaches. There is no such literature that correlates forming forces and power required in the metal forming process. In this research, the simulated power is estimated using the simulated forces (axial, radial, and tangential). The power is represented as torque multiplied by the angular velocity of the rollers. Here the angular velocity (ω) is considered as the 10.47 and 8.37 rad/sec for the feed speed ratio of 0.7 and 0.8 mm/rev, respectively. The perpendicular distance is assumed as the radial distance of the roller and the percentage of reduction. The total estimated power consumed during the flow forming process is given in equation (7). The estimated simulated power is compared with the experimental power, which is available in the literature [6].

The power consumed in the tangential direction is given as,

$$N_t = F_t \omega \sqrt{R\Delta h} \qquad (3)$$

The power consumed in the axial direction is given as,

$$N_z = F_z v \tag{4}$$

The power consumed in the radial direction is given as,

$$N_r = F_r \omega \sqrt{R\Delta h} \tag{5}$$

The total resultant power is given as,

$$N_{tot} = N_r + N_t + N_z \tag{6}$$

$$N_{tot} = F_t \omega \sqrt{R\Delta h} + F_z v + F_r \omega \sqrt{R\Delta h} \tag{7}$$

where ω is the angular speed of rotation of rollers (rad/s), R= radius of the roller (mm), Δh=percentage of reduction, F_r, F_t, and F_z are the simulated radial, tangential and axial forces respectively. Nagaranjan et al. [6] concluded that the power of the process depends on the following factors such as feed, rotational speed, roller geometry, and raw materials. The friction factor has a significant effect on the forming forces, although Park et al. [29] concluded that it does not affect the power consumption. At a lower percentage reduction for feed speed ratio of (0.7 and 0.8) mm/rev, the significant deviation is observed between the simulated power and the experimental power [6]. At higher percentage reduction, for different feed speed ratios, the simulated power is close to the experimental power [6].

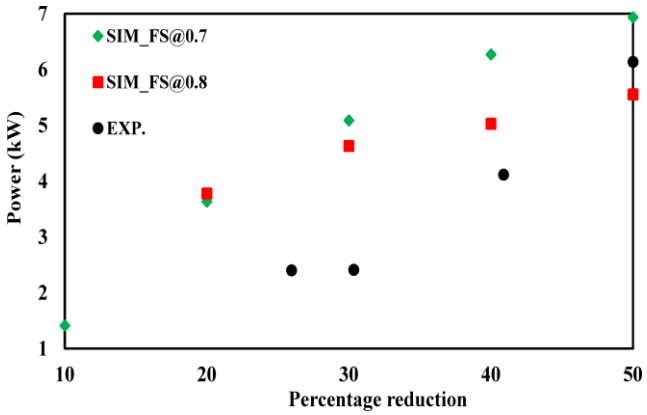

Fig.7. Comparison of power consumed between numerical results and experimental data

3.4 Determination of out of roundness

In the present research, out-of-roundness in a flow formed tube for different flow forming parameters are analyzed. The out of roundness is measured at different feed speed ratios and five different reduction percentages. The simulation was carried out for 5 seconds, so the simulated out of roundness is calculated for the beginning of the flow formed tube. Although this is a limitation of this research, it portrays the behavior of backward flow formed tubes. Each co-ordinates for each nodal point for circular cross-section was taken. Those co-ordinates were imported to the AutoCAD software, and the measurements were recorded. The simulated out of roundness is compared with the experimental data. The experiments are conducted for reduction percentages of 40, 50 at a feed speed ratio of 0.7 mm/rev, and 0.8 mm/rev, respectively. When the formed material flows along the circumferential direction rather than in the axial direction defects out of roundness occurs. The ovality is the difference between the maximum measured diameter to the minimum measured the diameter of flow formed tubes [30]. The ratio of circumferential to axial contact length provides a fair indication of out of roundness. Figure 8 shows the variation of entry angle with the ratio of circumferential (S) to axial (L) contact ratio (S/L ratio) at different feed speed ratios. From the Figure 8, it could be seen that the S/L ratio increases with the increase in entry angle. S/L >1 suggests deformation along the axial direction of the flow formed tubes. Thus, the out of roundness is influenced mainly by the geometry of the roller and feed speed ratio. From Figure 8, it could be seen that the ratio increases with a decrease in feed speed ratio. This is in line with the observation from Figure 9, where out of roundness is higher at lower feed speed ratio. The trends of experimental values and the simulated results are also in close agreement as both depicted an increase in the out of roundness with the rise in the percentage of reduction. The primary cause of out of roundness is that the deformed material is not constrained by any external objects. The deformed material on its course of deforming is only constrained by its surrounding material; hence, controlling along the free surface is difficult. This leads to out of roundness at the free end of the flow formed tube.

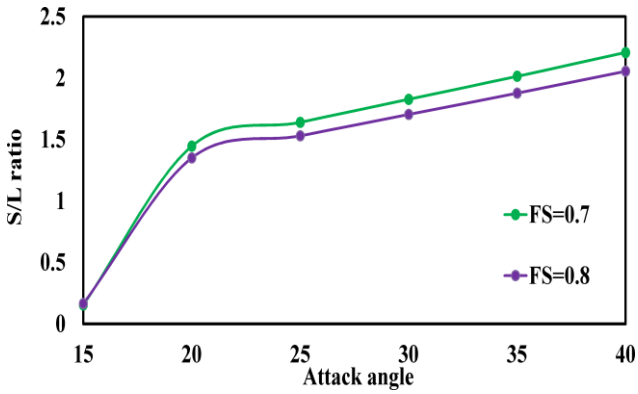

Fig.8. S/L ratio vs. percentage reduction at different feed-speed ratio (FS) at (0.7, 0.8) mm/rev

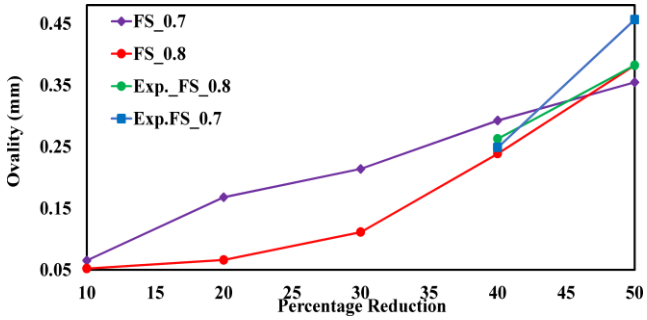

Fig. 9. Out of roundness in FE simulation vs. percentage reduction at a different feed-speed ratio (0.7 and 0.8) mm/rev

4. CONCLUSIONS

This study aimed to develop an FE model for three rollers backward flow forming process for AA6082 aluminum alloy. The following conclusion could be drawn from the current study.

Metal flow forming is an incremental forming process that can be vividly realized from the stresses that are only developed under the roller preform contact interface.

A comparison of components of roller forces with different existing theoretical models at different reduction was made. Among the three components of forming forces, the radial forces are the highest. The forming forces increase with an increase in feed speed ratio and percentage reductions. The simulated radial and axial forces are in close association with the theoretical model of Ma's [28]. The tangential forces showed a similar trend with the theoretical models discussed. The ratio of components of the simulated forces changes with the change in percentage reductions. The FE results were more practical, accurate than the existing theoretical models and hence, more acceptable.

Power consumed in FE based model bears close resemblance with the power from the experimental analysis. At feed speed ratio of 0.8 mm/rev for percentage reduction of (40 and 50), the simulated power of the flow forming process is close with the experimental power from the literature [6].

When the flow of the deformed material increases along the circumferential direction, out of roundness of the flow formed tube increases. At lower feed speed ratio, the out of roundness for flow formed tubes is more significant than at lower feed speed ratio. The out of roundness from FE based model at a feed speed ratio of 0.8 closely matches the experimental results using the same forming parameters as used in the FE model.

5. APPENDIX

(i) Different components of forces according to **Kobayashi and Thomsen's** algorithm

$$Fr = \frac{2}{\sqrt{3}}\sigma t_0 K_1 \sqrt{2R_p f \cot\alpha_p}$$

$$F_z = \frac{2}{\sqrt{3}}\sigma t_0 k_1 \sqrt{2R_p f \tan\alpha_p}$$

$$F_t = \frac{2}{\sqrt{3}}\sigma t_0 f k_2$$

$$k_0 = \frac{f}{t_0}\tan\alpha_p$$

$$K_1 = (1-\psi_t)[\frac{4}{3}(1-\sqrt{\frac{1-\psi_t}{K_0}}\tan^{-1}\sqrt{\frac{K_0}{1-\psi_t}}) + \frac{2}{9}\frac{K_0}{1-\psi_t} - (1+\frac{1}{3}\frac{K_0}{1-\psi_t})\ln(1-\psi_t+K_0)]$$

$$K_2 = \frac{1}{4K_0}\{(1-\psi_t+k_0)^2[1-2\ln(1-\psi_t+k_0)] - (1-\psi_t)^2[1-2\ln(1-\psi_t)]\}$$

(ii) Different components of forces according to **Thamasett's** algorithm

$$F_r = \frac{2}{\sqrt{3}}\Delta t\frac{\sigma}{\eta}\sqrt{R_i f \cot\alpha_p}$$

$$F_z = \frac{2}{\sqrt{3}}\Delta t\frac{\sigma}{\eta}\sqrt{R_i f \tan\alpha_p}$$

$$F_t = \frac{2}{\sqrt{3}}\Delta t f\frac{\sigma}{\eta}$$

$$R_i = \frac{2RR_p}{R+R_p}$$

(iii)Different components of forces according to **Chen et al.**

$$F_r = \frac{2}{\sqrt{3}}Kt_0\sigma\sqrt{fD_p\cot\alpha_p}$$

$$F_z = \frac{2}{\sqrt{3}}Kt_0\sigma\sqrt{fD_p\tan\alpha_p}$$

$$F_t = \frac{2}{\sqrt{3}}Kt_0 f\sigma$$

$$K = \ln\frac{1}{1-\psi_t}$$

(iv) Different components of forces according to **Ma's** algorithm

$$Fr = \frac{2}{\sqrt{3}}\sigma t_0\sqrt{fD_p\cot\alpha_p}(1+\psi_t)K$$

$$F_z = \frac{2}{\sqrt{3}}\sigma t_0\sqrt{fD_p\tan\alpha_p}(1+\psi_t)K$$

$$F_t = \frac{2}{\sqrt{3}}\sigma t_0 \mathrm{f}(1+\psi_t)K$$

$$K = [1+\sqrt{1-m^2}]\psi_t + [m\sqrt{fD\tan\alpha_p} + \sqrt{1-m^2}\, f \tan\alpha_p]/ (2t_0 - [m/\alpha_p + \sqrt{1-m^2}](\psi_t + \ln(1-\psi_t))$$

6. NOTATIONS

***FS*=** Feed speed ratio.
Ψ= Percentage reduction.
$\mathbf{t_0}$= initial wall thickness.
$\boldsymbol{\sigma}$= yield stress of the workpiece material.
f= feed rate.
$\boldsymbol{\alpha_p}$= enry angle of the roller.
$\boldsymbol{r_p}$=nose radius of the roller.
ψ_t = reduction in wall thickness.
Δt= real reduction in wall thickness.
$\boldsymbol{\eta}$ = deformation efficiency.
k= coefficient of spinning force.
$\boldsymbol{D_p}$= diameter of the roller.
m=friction factor of the friction versus shear resistance.

7. REFERENCE

1. Wong, C.C, Dean, T.A., Lin, J., (2003). *A review of spinning, shear forming and flow forming processes*, International Journal of Machine Tools & Manufacture, **43**(14), pp. 1419–1435.
2. Marini, D., Cunningham, D., Xirouchakis, P., Corney, J.R., (2016). *Flow forming: a review of research methodologies, prediction models and their applications*, International Journal of Mechanical Engineering and Technology, **7**(5), pp. 285–315.
3. Marini, D., Cunningham, D., Corney, J.R., (2015). *A review of flow forming processes and mechanisms, Key Engineering Materials*, **651-653**, pp. 750–758,.
4. Podder, B., Banerjee, P., Kumar, K.R., Hui, N.B., (2018). *Flow forming of thin walled precision shells*, Sådhanå, **43**, pp.1–16.
5. Hayama, M., Kudo, H., (1979). *Experimental study of tube spinning*, Bulletin of the JSME, **22**, pp.769–775.
6. Nagarajan, H. N., Kotrappa, H., Mallanna, C., (1981). *Mechanics of flow forming*, Annals of CIRP, **30**, pp. 159–162.
7. Singhal, R.P., Saxena P.K., Prakash, R., (1990). *Estimation of power in the shear spinning of long tubes in hard to work materials*, Journal of Materials Processing Technology, **23**, pp. 29–40.
8. Wong, C.C., Dean, T. A., Lin, J., (2004). *Incremental forming of solid cylindrical components using flow forming principles*, Journal of Material Processing Technology, **153-154**, pp. 60–66,.
9. F.A. Hua, Y.S. Yang, Y.N. Zhang, M.H. Guo, W.H. Tong, Z.Q. Hu, (2005). *Three-dimensional finite element analysis of tube spinning*, Journal of Material Processing Technology, **168**, pp.68–74.
10. Xia, Q.X., Cheng, X.Q., Hu, Y., Ruan, F., (2006). *Finite element simulation and experimental investigation on the forming forces of 3D non-axisymmetrical tubes spinning*, International Journal of Mechanical Sciences, **48**, pp.726–735.
11. Wong, C.C., Danno, A, Tong, K.K., Yong, M.S., (2008). *Cold rotary forming of the thin-wall component from flat-disc blank*, Journal of Material Processing Technology, **208**, pp.53–62.
12. Parsa, M.H., Pazooki, A.M., Ahmadabadi, M.N., (2009). *Flow forming and flow formability simulation*, The International Journal of Advanced Manufacturing Technology, **42**, pp. 463–473.
13. Razani, N.A.,.Agachai, A.J, Dariani, B.M., (2014). *Flow-forming optimization based on hardness of flow-formed AISI321 tube using response surface method*, International Journal of Advanced Manufacturing Technology, **70**, pp.1463–1471.
14. Wenchen, X., Zhao, X., Ma, H., Shan, D., Lin, H.,(2016). *Influence of roller distribution modes on spinning force during tube spinning*, International Journal of Mechanical Science, **113**, pp. 10–25.
15. Song, X.,.Fong, K.S, Oon, S.R., Tiong, W.R., Li, P.F., Korsunsky, A.M.., Danno, A., (2014). *Diametral growth in the forward flow forming process: simulation, validation and prediction*, International Journal of Advanced Manufacturing Technology, **71**, pp.207–217.
16. Gharehchah, H., Askar, M., Radmanesh, Z., (2014). *A study and FEM analysis of various parameters in flow forming of tubes*, Indian Journal of Scientific Research, **1**, pp.437–444.
17. Jafarzadeh. J., Sanei, S., (2014). Numerical and experimental study of feed rate as a process parameters in the flow forming of AA7075 solid tubes, Indian Journal Sci. Res., **2**, pp.151–159.
18. Bhatt. R.J., Raval, H.K., (2015). *Comparative study of forward and backward flow forming process using finite element analysis*, International Journal of Industrial Engineering and Management Science, **5**, pp. 46–49.
19. Shinde, H., Mahajan, P., Singh, A.K., Singh, R., Narasimhan, K., (2016). *Process modeling and optimization of the staggered backward flow forming process of maraging steel via finite element simulations*, International Journal of Advanced Manufacturing Technology, **87**(1), pp. 1851–1864.
20. Chen, Y., Clausen, A.H., Hoppersted, O.S., Langseth, M., (2009). *Stress strain behavior of aluminum alloys at a wide range of strain rates*, International Journal of Solids and Structures, **46**(21), pp. 3825–3835.
21. Kim, N. , Kim, H., Jin, K., (2013). *Minimizing the axial force and the material build-up in the tube flow forming process*, International Journal of Precision

Engineering and Manufacturing, **14**, pp. 259–266.
22. https://abaqus-docs.mit.edu/2017/English/ SIMA CAECAERefMap/simacae-t-itnhelpgeneralcontform. htm, Accessed on: 20th February, 2020.
23. https://abaqus-docs.mit.edu/2017/English /SIMA CAECAERefMap/simacae-m-ItnHelpSurftosurf- sb.h tm, Accessed on: 24 February 2020.
24. http://web.mit.edu/calculix_v2.7/CalculiX/ccx_2.7 /doc/ccx/ node27.html, Accessed on: 27th February 2020.
25. Kobayashi, S., Thomsen, E. G., (1962). *Theory of spin forging*, Ann CIRP, pp. 114–123.
26. Thamasett E., (1961). *Forces and deformations during ironing of cylindrical, rotationally symmetrical hollow bodies made of Aluminium*, TH Stuttgart.
27. Chen, K.X., Jia, W.D., Cao, G.S., (1986). *Process and equipment of power spinning process*, Press of National Defence Industry, pp.12.
28. Ma, Z.E., (1993). *Optimal Attack angle in tube spinning*, Journal of Material Process Technology, **37**, pp.217–224.
29. Park, J.W., Kim, Y.H., Bae, W.B., (1997). *Analysis of tube-spinning processes by the upper-boundstream-function method*, JMPT, **66**, pp. 195-203.
30. Podder, B., Banerjee, P., Kumar, K.R., Hui, N.B., (2019). *Study of the influences of process parameters on cold flow forming of al-tubes*, International Journal of Modern Manufacturing Technologies, **11**, pp. 95-106.

Received: March 18, 2021 / Accepted: June 15, 2021 / Paper available online: June 20, 2021